



HAL
open science

Modélisation numérique et expérimentale d'un système mécanique non-régulier à un degré de liberté

Solène Kojtych, Yann Colaïtis, Elsa Piollet, Alain Batailly

► To cite this version:

Solène Kojtych, Yann Colaïtis, Elsa Piollet, Alain Batailly. Modélisation numérique et expérimentale d'un système mécanique non-régulier à un degré de liberté. Congrès CSME-CFDSC 2019, Jun 2019, London, Canada. hal-02060883v2

HAL Id: hal-02060883

<https://hal.science/hal-02060883v2>

Submitted on 18 Mar 2019

HAL is a multi-disciplinary open access archive for the deposit and dissemination of scientific research documents, whether they are published or not. The documents may come from teaching and research institutions in France or abroad, or from public or private research centers.

L'archive ouverte pluridisciplinaire **HAL**, est destinée au dépôt et à la diffusion de documents scientifiques de niveau recherche, publiés ou non, émanant des établissements d'enseignement et de recherche français ou étrangers, des laboratoires publics ou privés.

Experimental and numerical modelling of a one-degree of freedom non-smooth mechanical system

S. Kojtych¹, Y. Colaitis¹, E. Piollet¹, A. Batailly¹

Abstract

The aim of this paper is to highlight some numerical challenges occurring in the analysis of non-smooth mechanical systems by focusing on a single degree of freedom system with unilateral contact interface. An experimental setup is developed, its vibration behaviour is analyzed both with and without contact interface by means of forward and backward sweep tests. The parameters of the associated numerical model are carefully identified based on experimental measurements and observations. Numerical investigations are carried out assuming the system's response is periodic using the harmonic balance method. Numerical results are then confronted to experimental observations: frequency response curves and time responses are superimposed in order to assess the accuracy of the numerical model. Overall, a good agreement is obtained between numerical predictions and experimental measurements. Additionally, the sensitivity of accelerations computed with the harmonic balance method to the Gibbs phenomenon is highlighted.

Keywords

non-smooth system; unilateral contact; harmonic balance method; experimental setup; Gibbs phenomenon

1 - Department of Mechanical Engineering, École Polytechnique de Montréal, P.O. Box 6079, Succ. Centre-Ville, Montréal, Québec, Canada H3C 3A7

Modélisation numérique et expérimentale d'un système mécanique non-régulier à un degré de liberté

S. Kojtych¹, Y. Colaitis¹, E. Piollet¹, A. Batailly¹

Résumé

Cet article a pour objectif de mettre en évidence certains défis numériques relatifs à l'analyse de systèmes mécaniques non-réguliers. Il se focalise sur l'étude d'un système mécanique à un degré de liberté avec interface de contact. Un banc d'essais spécifique a été conçu pour cette étude, son comportement vibratoire est tout d'abord analysé avec et sans interface de contact en effectuant des balayages en fréquence montant et descendant. Ces observations et mesures expérimentales servent de base pour la calibration des paramètres du modèle numérique associé. L'étude du modèle numérique est effectuée en supposant que le système a un comportement périodique à l'aide de la méthode de l'équilibrage harmonique. La confrontation des résultats numériques aux mesures expérimentales est faite en superposant des courbes de réponse en fréquence et des réponses temporelles obtenues expérimentalement et numériquement. Dans l'ensemble, une bonne superposition des résultats est observée. L'intérêt de cette confrontation réside notamment dans la mise en évidence de sensibilité numérique du calcul des accélérations par la méthode d'équilibrage harmonique. En effet, l'apparition du phénomène de Gibbs perturbe significativement les résultats dans le domaine fréquentiel.

Mots-clés

système non-régulier; contact unilatéral; méthode de l'équilibrage harmonique; dispositif expérimental; phénomène de Gibbs

1 - Département de génie mécanique, École Polytechnique de Montréal, P.O. Box 6079, Succ. Centre-Ville, Montréal, Québec, Canada H3C 3A7

Introduction

The modelling of non-smooth mechanical systems, particularly those featuring contact interfaces, is a challenge both from an experimental and a numerical standpoint. In a context where the design of sophisticated engineering applications now requires to account for inherent nonlinearities associated to contact [1, 2] or friction [3], the understanding of the physical phenomena at play is critical. Non-smooth mechanical systems are nonlinear systems characterized by the fact that their speed and acceleration fields are discontinuous. Because there is no equivalent to modal analysis in a non-smooth context, acquiring the intrinsic signature of a sophisticated mechanical non-smooth system is a very active field of research [4, 5]. Engineers and designers rely on several types of numerical methods [6, 7, 8] that may provide accurate results but that are also prone to numerical sensitivity or instability. The development of a robust numerical strategy thus requires that attention be paid to both physical and numerical aspects [1, 9].

In this context, and as a first step towards the development of a robust numerical strategy dedicated to the analysis of non-smooth mechanical systems, this paper presents a numerical/experimental confrontation on an academic non-smooth system: a one-degree of freedom setup featuring a contact interface. Based on the assumption that the system's response is periodic, numerical investigations are carried out using the Harmonic Balance Method (HBM). Though fairly simple, the mechanical system of interest exhibits a rich dynamic behaviour calling for a careful analysis of both experimental observations and numerical results. The numerical sensitivity of the HBM is underlined, particularly when looking at acceleration fields. Nonetheless, the HBM advantageously provides a qualitative view of the system's dynamics that time integration techniques—also considered in this paper for the sake of validation—fail to provide.

The second section of the article describes the experimental setup. An analytic model for the underlying smooth system is proposed before its key mechanical parameters are identified. Frequency sweep tests are conducted for two distinct experimental configurations: with and without the contact interface. The third section of this paper briefly describes the theory behind the HBM. A comparison between numerical and experimental results for the two experimental configurations is presented and the differences are discussed. The influence of the number of harmonics taken into account in the HBM on the accuracy of the predicted solutions is investigated.

1. Experimental system

1.1 Setup description

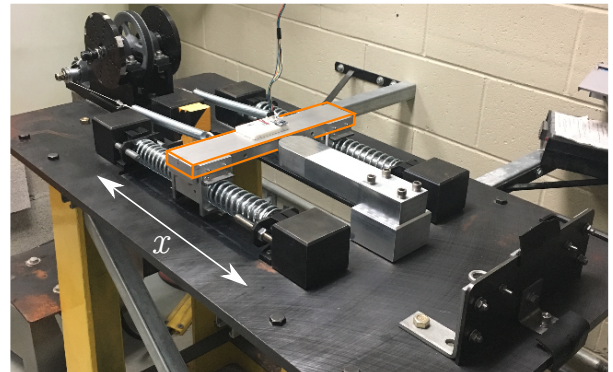
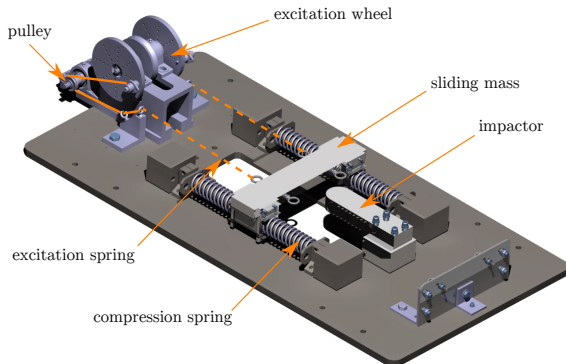


Figure 1. CAD and photo of the experimental setup.

The experimental setup depicted in Fig. 1 aims at modelling a one-degree of freedom mass-spring system with contact-induced nonlinearity. The system consists of two main bodies: a sliding mass, excited along the x axis, and an impactor fixed on the bench structure and constraining the displacement of the mass. The impactor may be removed, thus making it possible to identify parameters of the system without contact interface. The impactor is made of steel, the gap between its extremity and the sliding mass at rest is $L = 10$ mm. The semi-cylindrical

extremity of the impactor yields a line-to-surface contact interface. The sliding system is designed to meet specific criteria while the bench support and excitation system are adapted from [10].

Sliding system The sliding mass is made of steel, it is guided along the x direction by two parallel shafts fixed on the bench support. Sliding is made possible by two linear self-aligning bearings which also reduce friction with the shafts. Four compression springs of stiffness k_c placed along the guiding shafts allow the mass to oscillate. An initial compression of these springs ensures permanent contact with the mass in operation.

Excitation system A sinusoidal excitation is applied on the sliding system. A motor (not visible in Fig. 1) is fixed below the bench support, it provides a rotary motion which is transmitted to an excitation wheel. Two eccentric pins on this wheel are linked with two extension springs by means of a cable-pulley system. Finally, the sliding system undergoes a translation motion initiated by the springs. The magnitude of the excitation force depends on the stiffness k_e of the excitation springs and the excitation frequency can be chosen by the control panel of the motor and goes from about $0.85f_0$ to $1.15f_0$, where f_0 is the system's natural frequency. It is assumed that the global stiffness of the system is not significantly impacted by the excitation springs stiffness, because their contribution are very low compared to compression springs.

Measurement system A $\pm 16 g$ triple-axis accelerometer fixed on the mass is used to acquire accelerations and for transmission to a data acquisition system (DAQ). For cost-efficient reasons as well as academic purposes, the use of an ADXL326 accelerometer from Analog Devices and an Arduino UNO microcontroller (revision 3) as DAQ is considered in this study. The DAQ behavior is implemented through codes in C programming language, pre- and post-processing operations are carried out automatically by means of a dedicated Python 2 interface developed specially for the experiment. Both the accelerometer and the DAQ were calibrated prior to the experiments. All codes are open source and available online [11]. The resolution of the measurement system is $0.05 g$ and the sampling frequency is set to 1000 Hz.

1.2 Model and parameters identification

Assuming the investigated mechanical system behaves as a one-degree of freedom system, its equation of motion is given by:

$$m\ddot{x} + d(\dot{x}) + kx = F(\omega, x, t) \quad (1)$$

where m and k are respectively the mass and the global stiffness of the system, $d(\dot{x})$ is a damping function to be determined, F stands for the external force, ω is the pulsation of the excitation and t is the time.

The aim of this section is to introduce and quantify sources of uncertainty for each of the system parameters m , $d(\dot{x})$, k and F in order to identify a suitable value for each of them. A precise estimation of F is particularly arduous to obtain as a non-negligible transverse motion of the extension springs is observed experimentally. For this reason, the characterization of the system follows a two-pronged approach: (1) values of m , d and k are first obtained without any excitation ($F = 0$) then, (2) F is identified.

Stiffness identification An uniaxial load frame is used to obtain an accurate value of the static stiffnesses of both compression and extension springs. The measurements confirmed the linear behavior of the springs. Averaged stiffnesses are summed up in Tab. 1 and the global stiffness of the system is given by:

$$k = 4k_c + 2k_e. \quad (2)$$

Due to the fairly low excitation frequency $f_e \approx 13$ Hz, a characterization of dynamical stiffnesses is assumed unnecessary.

Mass identification Although the mass of each component is known, a precise estimate of the mass of the sliding system is difficult to assess due to the unknown contribution of compression springs to the global sliding system's mass m . Indeed, the mass of compression springs is distributed between the steel mass and the guiding shaft, thus only bounds can be given for m :

$$3.718 \text{ kg} \leq m \leq 4.612 \text{ kg} \quad (3)$$

A more accurate estimate of the system's mass calls for a thorough analysis of the free response of the system.

| quantity | expression | value |
|------------------------------|------------|-----------|
| compression spring stiffness | k_c | 6 278 N/m |
| excitation spring stiffness | k_e | 138 N/m |
| viscous damping coefficient | ξ | 0.014 |
| dry friction coefficient | μ | 0.135 |
| mass of sliding system | m | 4.262 kg |

Table 1. Parameters identified for the numerical model.

Damping analysis Looking at the test bench depicted in Fig. 1, it is assumed that structural damping may essentially result from friction in linear bearings and from losses within the springs. Free vibration decay is thus analyzed: the sliding mass is moved to $x = 10$ mm, it is then released and accelerations are recorded. This test is conducted three times for the sake of repeatability.

Three damping models are considered, see Tab. 2. Raw acceleration data depicted in Fig. 2 are properly filtered and converted into displacements in order to identify the best parameters for each model (μ and/or ξ). The best matching is observed with the mixed damping model (viscous damping ξ and dry friction μ) which yields very good agreement with experimental data as shown in Fig. 3. Averaged values of the best fit parameters μ and ξ for the three tests are given in Tab. 1.

The low value of ξ underlines that viscous damping is weak. For this reason, free-decay tests may be used to approximate the system's natural frequency $f_0 = 12.28$ Hz and thus determine its mass $m = 4.262$ kg. Values of m , k_c , k_e , ξ and μ —which define the left term of (1)—used for the numerical model are reported in Tab. 1.

| damping model | equation |
|----------------------------------|--|
| viscous damping | $d(\dot{x}) = 2m\xi\omega_0\dot{x}$ |
| dry friction | $d(\dot{x}) = \mu mg \operatorname{sgn}(\dot{x})$ |
| viscous damping and dry friction | $d(\dot{x}) = 2m\xi\omega_0\dot{x} + \mu mg \operatorname{sgn}(\dot{x})$ |

Table 2. Damping model equations ($g = 9.81$ m/s² gravitational constant, $\operatorname{sgn}()$ sign function, ξ viscous damping coefficient, μ dry friction coefficient, $\omega_0 = 2\pi f_0$ natural pulsation of the system).

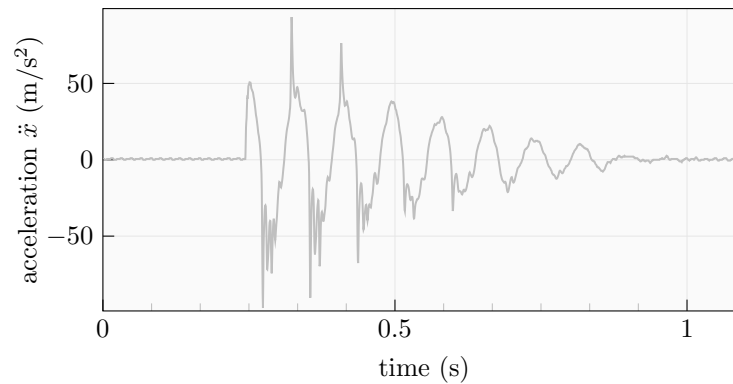


Figure 2. Free decay experimental data.

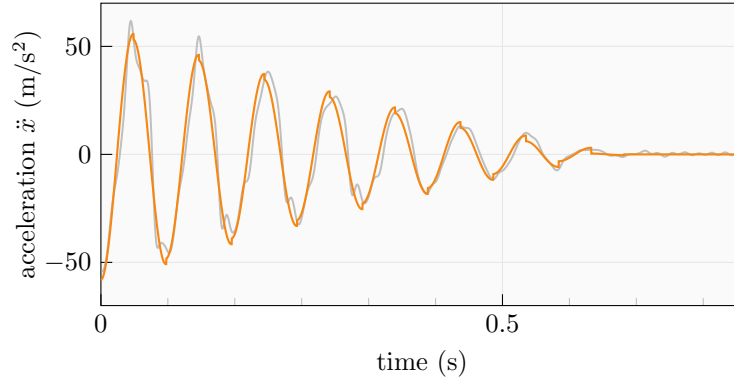


Figure 3. Simulation of damping model with viscous damping and dry friction (—) and experimental acceleration data (—).

Frequency analysis A frequency sweep is conducted to determine the frequency response of the system as well as the expression of the right term of (1). The excitation frequency is updated step-by-step; for each increment the amplitude of the system's steady state response is recorded. Acquisitions last for 20 s and are recorded at a frequency rate of 1000 Hz. The close agreement of successive sweep tests has been checked in order to ensure the repeatability of the procedure. Only results for a single sweep test are presented in the following paragraphs.

In order to improve the experimental measurements accuracy, the frequency step is decreased to 0.05 Hz in the vicinity of the resonance peak. For each frequency excitation value, the maximal magnitude is plotted to draw an experimental response curve, see Fig. 4. Tests were made both for forward and backward frequency sweeps: the good match between the two responses underlines that the system without impactor does not exhibit any unwanted nonlinearity.

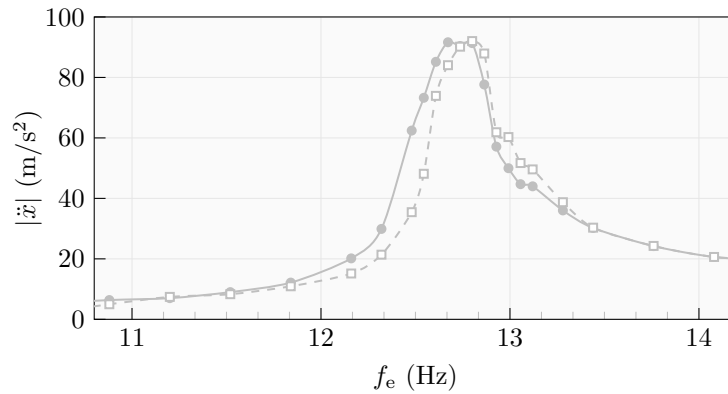


Figure 4. Experimental frequency response for the system without impactor: forward (●) and backward (□) frequency sweeps.

High-resolution video-tracking used during the sweep tests shows that the excitation springs undergo large frequency-dependent transverse displacements in operation as depicted in Fig. 5. As a consequence, it is not possible to establish any straightforward relation between the excitation springs stiffness and the magnitude of the force F . Due to the fact that the excitation is driven by the rotary motion of the motor, it is assumed that the right term of (1) may be written as:

$$F(\omega, x, t) = f_{\text{ext}}(\omega, t) = F(\omega) \sin(\omega t) \quad (4)$$

where $\omega = 2\pi f_e$ is the pulsation of the excitation and $F(\omega)$ the unknown force magnitude.

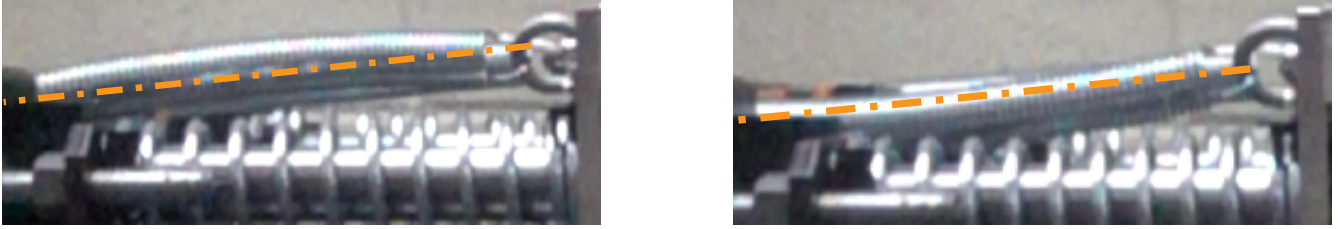


Figure 5. Extreme positions of an excitation spring undergoing transverse displacement in operation : (---) theoretical baseline.

Through a computation of the system's forced response using the previously identified parameters m , $d(\dot{x})$ and k , the values of $F(\omega)$ that corresponds to the experimentally measured amplitudes are retrieved for each considered excitation frequency. $F(\omega)$ related to both forward (\bullet) and backward (\square) frequency sweeps are pictured in Fig. 6. The similarity of the curves attest that the calculated excitation force can be considered as independent from the type of sweep.

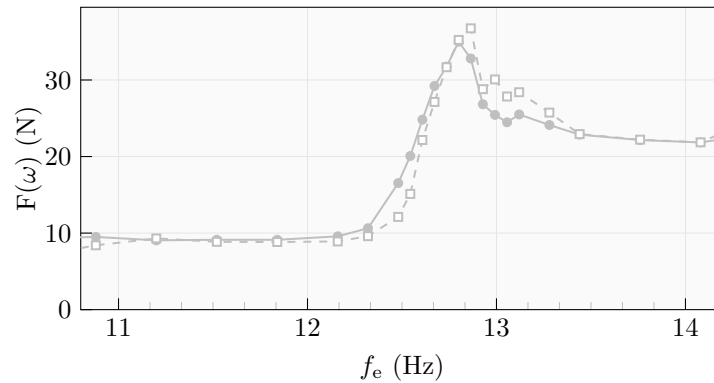


Figure 6. Magnitude of the excitation force obtained for forward (\bullet) and backward (\square) frequency sweeps.

1.3 Experimental results for system with impactor

Forward and backward sweep tests are conducted with impactor. Results in acceleration are depicted in Fig 7 and superimposed with experimental results without impactor. Curves are significantly different: for the forward sweep, the highest magnitude is located at a higher frequency than for the backward sweep and a jump in magnitude is visible at about 13.5 Hz. These behaviours are typical of the contact stiffening phenomenon and attest that a strong nonlinearity is induced by the contact interface. The slight decrease in magnitude for the three excitation points located immediately before the jump is assumed to result from a slight rotary motion of the sliding mass, due to unavoidable clearances in the linear bearings. A more in-depth analysis of the influence of this potential second degree of freedom goes beyond the scope of this study.

2. Numerical model

Several numerical strategies may be employed to solve (1). In particular, one may distinguish two classes of methods: (1) time integration and (2) frequency methods. Time integration is costly but advantageously does not rely on any assumption with respect to the system's behaviour; it is still commonly used today in the industry. To the contrary, frequency methods typically rely on an assumption of periodicity but may provide fast and reliable results. More importantly, frequency methods such as the HBM, when coupled to continuation algorithms, are able to provide a qualitative view of the system's dynamics which is key for understanding the underlying physical phenomena.

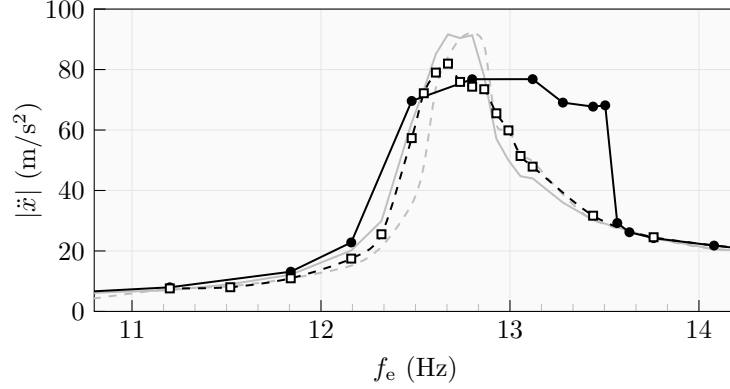


Figure 7. Experimental frequency response for the system with impactor: forward (●) and backward (□) frequency sweeps.

2.1 Theoretical presentation of the harmonic balance method

The HBM is widely used for the computation of nonlinear mechanical problems' periodic solutions [12, 13]. It relies on the assumption that the solution of a nonlinear system (1) undergoing a harmonic forcing (4) may be approximated by a truncated Fourier series up to the H -th harmonic:

$$x(t) \simeq \frac{a_0}{\sqrt{2}} + \sum_{j=1}^H [a_j \cos(j\omega t) + b_j \sin(j\omega t)] \quad (5)$$

where a_j and b_j are the unknowns Fourier coefficients related to cosine and sine terms. The same decomposition may also be used for the nonlinear forces f_{nl} (e.g. contact or friction) and the periodic external force f_{ext} :

$$\begin{aligned} f_{nl}(x, \dot{x}) &\simeq \frac{a_0^{nl}}{\sqrt{2}} + \sum_{j=1}^H [a_j^{nl} \cos(j\omega t) + b_j^{nl} \sin(j\omega t)] \\ f_{ext}(\omega, t) &\simeq \frac{a_0^{ext}}{\sqrt{2}} + \sum_{j=1}^H [a_j^{ext} \cos(j\omega t) + b_j^{ext} \sin(j\omega t)]. \end{aligned} \quad (6)$$

From this point, all the Fourier coefficients may be gathered into the $(2H + 1)$ -dimensional vectors:

$$\begin{aligned} \tilde{\mathbf{x}} &= [a_0 \ a_1 \ b_1 \ \dots \ a_H \ b_H]^T \\ \tilde{\mathbf{f}}_{nl} &= [a_0^{nl} \ a_1^{nl} \ b_1^{nl} \ \dots \ a_H^{nl} \ b_H^{nl}]^T \\ \tilde{\mathbf{f}}_{ext} &= [a_0^{ext} \ a_1^{ext} \ b_1^{ext} \ \dots \ a_H^{ext} \ b_H^{ext}]^T \end{aligned} \quad (7)$$

where the symbol ($\tilde{\cdot}$) refers to frequency domain variables. By defining the Fourier basis vector \mathbf{T}_H related to (5):

$$\mathbf{T}_H = \left[\frac{1}{\sqrt{2}} \cos(\omega t) \ \sin(\omega t) \ \dots \ \cos(H\omega t) \ \sin(H\omega t) \right], \quad (8)$$

(5) and (6) are now read as:

$$\begin{aligned} x(t) &= \mathbf{T}_H \tilde{\mathbf{x}} \\ f_{nl}(x, \dot{x}) &= \mathbf{T}_H \tilde{\mathbf{f}}_{nl} \\ f_{ext}(\omega, t) &= \mathbf{T}_H \tilde{\mathbf{f}}_{ext}. \end{aligned} \quad (9)$$

Also, velocities and accelerations may be written as:

$$\begin{aligned}\dot{x}(t) &= \dot{\mathbf{T}}_H \tilde{\mathbf{x}} = \omega(\mathbf{T}_H \nabla) \tilde{\mathbf{x}} \\ \ddot{x}(t) &= \ddot{\mathbf{T}}_H \tilde{\mathbf{x}} = \omega^2(\mathbf{T}_H \nabla^2) \tilde{\mathbf{x}}\end{aligned}\quad (10)$$

where ∇ is a derivative operator defined as:

$$\nabla = \begin{bmatrix} 0 & & & & \\ & \ddots & & & \\ & & \nabla_j & & \\ & & & \ddots & \\ & & & & \nabla_H \end{bmatrix} \quad \text{and} \quad \nabla^2 = \nabla \nabla \quad (11)$$

with

$$\nabla_j = j \begin{bmatrix} 0 & 1 \\ -1 & 0 \end{bmatrix} \quad \text{for } j = 1, \dots, H. \quad (12)$$

Using (9) and (10), the equation of motion (1) becomes:

$$m\omega^2(\mathbf{T}_H \nabla^2) \tilde{\mathbf{x}} + c\omega(\mathbf{T}_H \nabla) \tilde{\mathbf{x}} + k\mathbf{T}_H \tilde{\mathbf{x}} + \mathbf{T}_H \tilde{\mathbf{f}}_{\text{nl}} \simeq \mathbf{T}_H \tilde{\mathbf{f}}_{\text{ext}} \quad (13)$$

where $c = 2\xi\omega_0 m$ accounts for viscous damping. The difference between the left and right terms of (13) is related to the truncation of $x(t)$, see (5), it is called the residual $\mathbf{r}(\tilde{\mathbf{x}}, t)$ and can be expressed as:

$$\begin{aligned}\mathbf{r}(\tilde{\mathbf{x}}, t) &= m\omega^2(\mathbf{T}_H \nabla^2) \tilde{\mathbf{x}} + c\omega(\mathbf{T}_H \nabla) \tilde{\mathbf{x}} \\ &\quad + k\mathbf{T}_H \tilde{\mathbf{x}} + \mathbf{T}_H \tilde{\mathbf{f}}_{\text{nl}}(\tilde{\mathbf{x}}) - \mathbf{T}_H \tilde{\mathbf{f}}_{\text{ext}}(\omega, t).\end{aligned}\quad (14)$$

A Galerkin projection [6] on the Fourier basis \mathbf{T}_H is then applied to remove the time dependency of $\mathbf{r}(\tilde{\mathbf{x}}, t)$ so as to obtain a relation between the unknowns, a_j and b_j . This leads to the following set of nonlinear algebraic equations:

$$\begin{aligned}\mathbf{R}(\tilde{\mathbf{x}}, \omega) &= m\omega^2 \nabla^2 \tilde{\mathbf{x}} + c\omega \nabla \tilde{\mathbf{x}} + k\mathbf{I}_{2H+1} \tilde{\mathbf{x}} \\ &\quad + \mathbf{I}_{2H+1} \tilde{\mathbf{f}}_{\text{nl}}(\tilde{\mathbf{x}}) - \mathbf{I}_{2H+1} \tilde{\mathbf{f}}_{\text{ext}}(\omega)\end{aligned}\quad (15)$$

with \mathbf{I}_{2H+1} the identity matrix of size $(2H + 1)$. Equation (15) may be written in a more compact form:

$$\mathbf{R}(\tilde{\mathbf{x}}, \omega) = \mathbf{Z}(\omega) \tilde{\mathbf{x}} + \tilde{\mathbf{f}}_{\text{nl}}(\tilde{\mathbf{x}}) - \tilde{\mathbf{f}}_{\text{ext}}(\omega) = 0 \quad (16)$$

where $\mathbf{Z}(\omega)$ is the square linear dynamic stiffness matrix of size $(2H + 1)$ defined by:

$$\mathbf{Z}(\omega) = m\omega^2 \nabla^2 + c\omega \nabla + k\mathbf{I}_{2H+1}. \quad (17)$$

The nonlinear algebraic system (16) may be solved iteratively, for instance with a Newton-type or jacobian-free algorithms [12].

Nonlinear forces In general, the expression of the external forcing $\tilde{\mathbf{f}}_{\text{ext}}$ is known. Nonlinear forces $\tilde{\mathbf{f}}_{\text{nl}}$ however depend on the displacement and velocity amplitudes and are not known *a priori*. In order to address this issue, an Alternating Frequency/Time (AFT) procedure is adopted [14, 13]. It consists in the use of direct and inverse Discrete Fourier Transform (DFT) to evaluate the expression of nonlinear forces $f_{\text{nl}}(x, \dot{x})$ as well as their derivatives $\frac{\partial f_{\text{nl}}}{\partial x}$, $\frac{\partial f_{\text{nl}}}{\partial \dot{x}}$ in the time domain, then to obtain the frequency domain representations of $\tilde{\mathbf{f}}_{\text{nl}}$ and $\frac{\partial \tilde{\mathbf{f}}_{\text{nl}}}{\partial \tilde{\mathbf{x}}}$ (the latter is only required for a Newton nonlinear solver). The AFT procedure may be illustrated as follows:

$$\tilde{\mathbf{x}} \xrightarrow{\text{DFT}^{-1}} x(t), \dot{x}(t) \longrightarrow f_{\text{nl}}(x(t), \dot{x}(t)) \xrightarrow{\text{DFT}} \tilde{\mathbf{f}}_{\text{nl}}(\tilde{\mathbf{x}}) \quad (18)$$

In this study a distinction is made between the normal f_n and tangential f_t components of the nonlinear forces, respectively related to contact and dry friction. An exponential penalty law is employed to model unilateral contact constraints:

$$f_n = \begin{cases} 0 & \text{if } \delta \leq -c_0 \\ \frac{f_0}{e^{(1)}-1} \left[\left(\frac{\delta}{c_0} + 1 \right) \left(e^{\left(\frac{\delta}{c_0} + 1 \right)} - 1 \right) \right] & \text{if } \delta > -c_0 \end{cases} \quad (19)$$

where δ is the penetration between solids, and (c_0, f_0) are contact regularization parameters. With respect to dry friction, the computation of f_t relies on a regularized Coulomb law:

$$f_t = \mu mg \operatorname{sgn}(\dot{x}) \simeq \mu mg \tanh(\gamma \dot{x}) \quad \text{with } \gamma \gg 1 \quad (20)$$

where γ is the sign function regularization parameter.

The choice of parameters c_0 , f_0 and γ is based on a compromise between an accurate modelling of the physical problem and the need to ensure numerical stability. In this study, $c_0 = 5 \times 10^{-4}$ m, $f_0 = 10$ N and $\gamma = 10$ are used. **Path following : continuation** Nonlinear dynamics systems often exhibit complex behaviours, such as coexistence of multiple solutions. The possibility to obtain some of these distinct solutions is a key asset of the HBM in comparison with time integration techniques. To this end, an arc-length continuation procedure is combined with the HBM/AFT algorithm. It consists in a prediction-correction approach to build the frequency response curve where ω is unknown and constrained by a curvilinear abscissa parametrization of the curve. For the sake of brevity, details of this algorithm are not given in this paper, the reader may refer to [15] for more details.

2.2 Numerical simulations without contact interface

Without contact interface, it is assumed that dry friction is the only source of nonlinearity:

$$f_{nl}(x, \dot{x}) = f_t. \quad (21)$$

Experimental data and numerical frequency response curves for the identified set of parameters given in Tab. 1 are presented in Fig. 8. Both forward and backward frequency sweeps are considered numerically and experimentally. A good agreement between HBM calculations and experimental values is evidenced as numerical predictions are almost perfectly superimposed with experimental measurements.

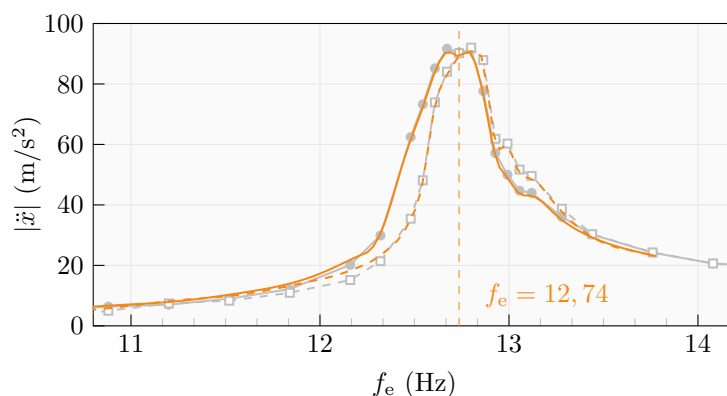


Figure 8. Comparison of experimental frequency response curves (forward (●) and backward (□) frequency sweeps) to the HBM model with $H = 8$ (forward (—) and backward (---) frequency sweeps).

When looking at the response of the system in the time domain at the resonance peak, see Fig. 9, it appears that the numerical prediction matches experimental observation. In addition to experimental data and HBM results,

the solution obtained using time integration (an embedded Runge-Kutta RK5 (4) time integration scheme is used) is also plotted in order to ensure the validity of numerical calculations. To give an idea, HBM computation time for one solution is about less than one second, and for time integration is about 1-2 minutes. As mentioned above, it is assumed that the minor discrepancy between numerical results and experimental observations in the vicinity of the highest amplitudes in Fig. 9 is related to a minor rotation of the mass due to bearing clearances.

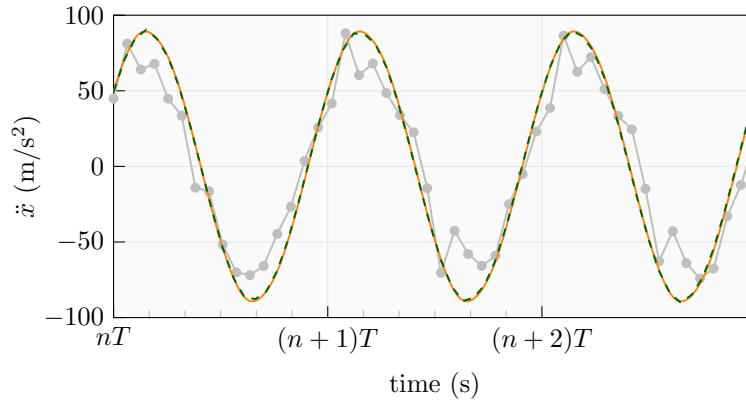


Figure 9. Comparison between experimental acceleration evolution (forward frequency sweep (●)), HBM (—) with $H = 8$, and RK5 (4) time integration (- - -) at $f_e = 12.74$ Hz.

2.3 Numerical simulations with contact interface

Accounting for the contact interface, the nonlinear forces may be written as:

$$f_{nl}(x, \dot{x}) = f_n + f_t. \quad (22)$$

The superimposition of results obtained with the HBM considering $H = 20$ harmonics and experimental measurements is given in Fig. 10. Significant differences of amplitudes are found between the numerical prediction (—) and

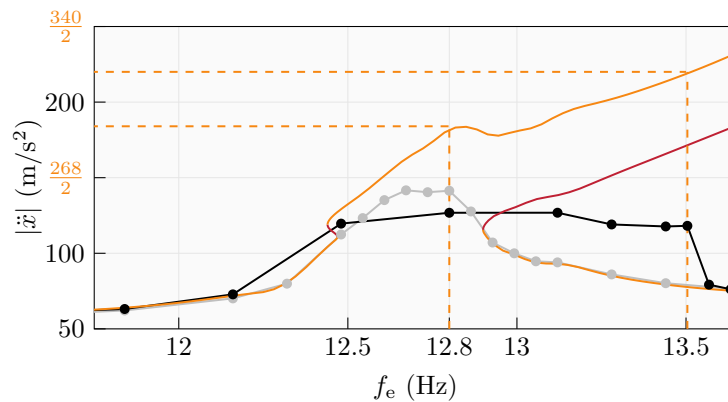


Figure 10. Comparison between experimental frequency response for the system : without impactor (●), with impactor (forward frequency sweep (●)) and HBM (stable (—), unstable (—) periodic solutions) with $H = 20$.

and experimental measurements (—). It is noticeable that the discrepancy between the two plots increases as the excitation frequency increases. In order to better understand the root cause of such discrepancy, time

responses predicted numerically and observed experimentally are superimposed for two distinct excitation frequencies: $f_{e1}, f_{e2} = 12.8, 13.5$ Hz. The comparison between experimental and numerical accelerations are presented in Figs. 11 and 12. Interestingly, numerical predictions and experimental measurements essentially differ over a very narrow

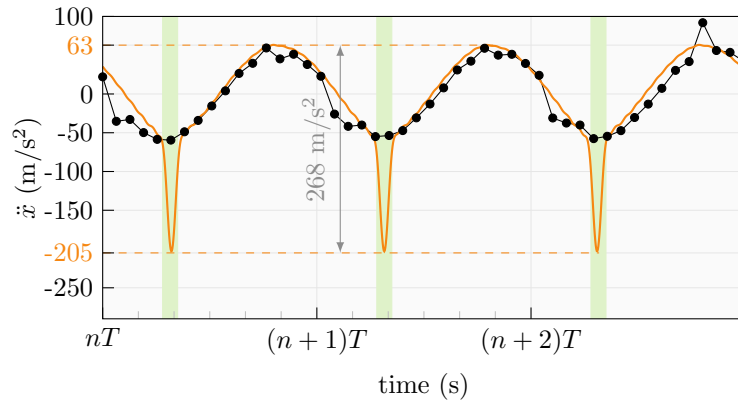


Figure 11. Comparison between experimental acceleration evolution (forward frequency sweep (●)) and HBM (—) with $H = 20$ at $f_{e1} = 12.8$ Hz. Time interval over which contacts occur is highlighted in green.

time frame, corresponding to the exact instant over which contact with the impactor occurs. During the contact phase, HBM results present a large peak of amplitude which is responsible for the error in amplitude evidenced in Fig. 10. The direct comparison of Figs. 11 and 12 underlines that the amplitude of this peak increases with the excitation frequency.

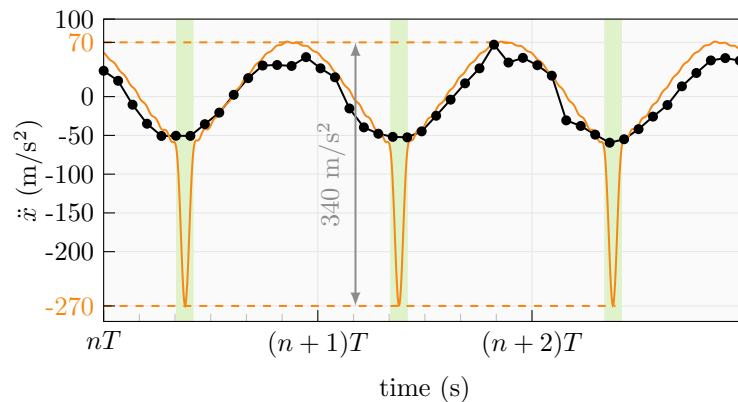


Figure 12. Comparison between experimental acceleration evolution (forward frequency sweep (●)) and HBM (—) with $H = 20$ at $f_{e2} = 13.5$ Hz. Time interval over which contacts occur is highlighted in green.

The solutions computed by HBM at $f_e = 12.8$ Hz for different values of the number of harmonics H —not shown in this paper due to a lack of space—underline that the amplitude of the peak is strongly influenced by the number of harmonics H thus indicating it is essentially a numerical artifact. The well-known Gibbs phenomenon is responsible for this peak: in the vicinity of the time over which contacts occur, speeds and accelerations are non-differentiable and the Fourier basis used in (5) becomes ill-suited to accurately represent time responses.

There exists strategies to mitigate the Gibbs phenomenon, including the use of different bases of functions, see for instance [8]. One may note that the definition of the acceleration given in (10) in the frequency domain is proportional to ω^2 . For this reason, accelerations are particularly sensitive to the Gibbs phenomenon since the

excitation frequency acts as a quadratic error amplification factor. To the contrary, results in terms of displacements, which are not displayed for the sake of brevity do not feature such discrepancy with experimental results. One way to mitigate the influence of the Gibbs phenomenon on the numerical results is to make a truncation of the predicted numerical solution computed for $H = 20$ to a lower number of harmonics; such truncations are depicted in Fig. 13. It is noticeable that the truncation of the solution to its first harmonic yields an acceptable approximation of the experimental observation.

Finally, the amplitude of all numerical solutions computed with $H = 20$ and truncated to their first harmonic (—) are plotted in Fig. 14. There is a better agreement between the numerically predicted frequency response of the system and experimental observations throughout the frequency range of interest. One should note that these solutions are distinct from the solutions directly computed by HBM with $H = 1$ (---), also depicted in Fig. 14.

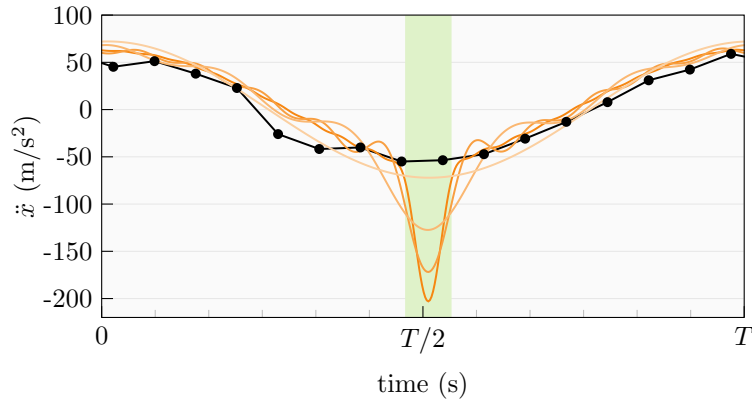


Figure 13. HBM results at $f_{e1} = 12.8$ Hz : full solution with $H = 20$ (—) and truncations to the first: 10 harmonics (—), 5 harmonics (—) and 1 harmonic (—).

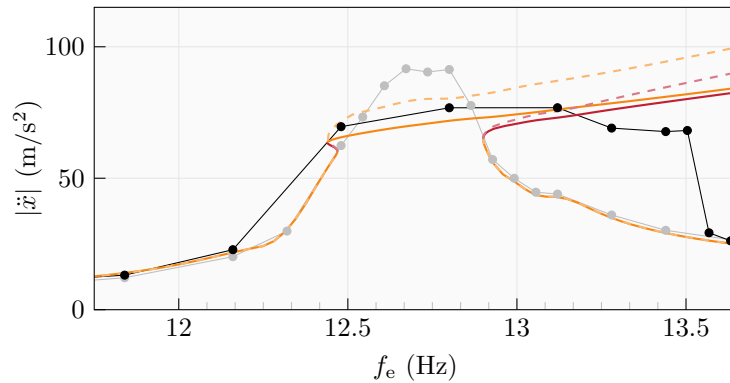


Figure 14. Frequency responses: experiment without impactor (\bullet), with impactor (\bullet), HBM (—) with $H = 20$ truncated to the first harmonic, and HBM (---) with $H = 1$.

3. Conclusion

The numerical and experimental modelling of a single degree of freedom mechanical system with contact interface is investigated in this study. Based on a newly designed experimental setup, the mechanical parameters of the associated numerical model are identified. Frequency sweep tests are conducted with and without the contact

interface. Assuming the periodicity of the system's response, the HBM is used to predict vibrations of the system. A good agreement is found between numerical prediction and experimental results in both time and frequency domains. Moreover, this study highlights the sensitivity of numerical results to the Gibbs phenomenon, particularly when looking at the accelerations.

This article underlines challenges in design and analysis of non-smooth one-degree of freedom mechanical system and attests to the importance of numerical/experimental confrontation. Future work will focus on an in-depth analysis of experimental data in displacements as well as investigations on the stability of experimental solutions prior to the jump discontinuity in forward frequency sweep. From a numerical standpoint, work is in progress for including within the HBM a numerical procedure of wear management in order to simulate complex industrial systems featuring wear and fretting.

Acknowledgments

This research was supported by the Fonds de Recherche du Québec – Nature et Technologies (FRQ-NT) and the Natural Sciences and Engineering Research Council of Canada (NSERC). The authors would like to thank Charles Audet (Polytechnique Montréal) for comments and careful proofreading that helped improve the manuscript. The authors also thank Samuel Tremblay and Pierre Brault-des-Grouets for their help with the design and the setting of the experimental setup.

References

- [1] Batailly, A., Legrand, M., Millecamps, A., and Garcin, F., 2012. “Numerical-Experimental Comparison in the Simulation of Rotor/Stator Interaction Through Blade-Tip/Abradable Coating Contact”. *Journal of Engineering for Gas Turbines and Power*, **134**(8), June, pp. 082504–082504–11. doi: 10.1115/1.4006446 - oai: hal-00746632.
- [2] G. Jacquet-Richardet, M. Torkhani, P. Cartraud et. al, 2013. “Rotor to stator contacts in turbomachines. Review and application”. *Mechanical Systems and Signal Processing*, **40**(2), Nov., pp. 401–420. doi: 10.1016/j.ymssp.2013.05.010 - oai: hal-00934050.
- [3] Krack, M., Salles, L., and Thouverez, F., 2017. “Vibration Prediction of Bladed Disks Coupled by Friction Joints”. *Archives of Computational Methods in Engineering*, **24**(3), July, pp. 589–636. doi: 10.1007/s11831-016-9183-2 - oai: hal-01825517.
- [4] Noël, J., and Kerschen, G., 2017. “Nonlinear system identification in structural dynamics: 10 more years of progress”. *Mechanical Systems and Signal Processing*, **83**, Jan., pp. 2–35. doi: 10.1016/j.ymssp.2016.07.020.
- [5] Laxalde, D., and Thouverez, F., 2009. “Complex non-linear modal analysis for mechanical systems: Application to turbomachinery bladings with friction interfaces”. *Journal of Sound and Vibration*, **322**(4-5), May, pp. 1009–1025. doi: 10.1016/j.jsv.2008.11.044 - oai: hal-00343494.
- [6] Kim, W.-J., and Perkins, N., 2003. “Harmonic balance/Galerkin method for non-smooth dynamic systems”. *Journal of Sound and Vibration*, **261**(2), Mar., pp. 213–224. doi: 10.1016/S0022-460X(02)00949-5 - oai: hal-01693093.
- [7] Thorin, A., Delezoide, P., and Legrand, M., 2017. “Non-smooth modal analysis of piecewise-linear impact oscillators”. *SIAM Journal on Applied Dynamical Systems*, **16**(3), pp. 1710–1747. doi: 10.1137/16M1081506 - oai: hal-01298983.
- [8] Jones, S., and Legrand, M., 2014. “Forced vibrations of a turbine blade undergoing regularized unilateral contact conditions through the wavelet balance method”. *International Journal for Numerical Methods in Engineering*, **101**(5), Oct., pp. 35–374. doi: 10.1002/nme.4807 - oai: hal-00806545.
- [9] Issanchou, C., Bilbao, S., Carrou, J.-L. L., Touzé, C., and Doaré, O., 2017. “A modal-based approach to the nonlinear vibration of strings against a unilateral obstacle: Simulations and experiments in the pointwise case”. *Journal of Sound and Vibration*, **393**, pp. 229–251. doi: 10.1016/j.jsv.2016.12.025 - oai: hal-01461730v1.

- [10] Charreton, C., Béguin, C., Ross, A., Étienne, S., and Pettigrew, M., 2015. “Two-phase damping for internal flow: Physical mechanism and effect of excitation parameters”. *Journal of Fluids and Structures*, **56**, July, pp. 56–74. doi: 10.1016/j.jfluidstructs.2015.03.022 - oai: [hal-01223577](#).
- [11] Kojtych, S., 2019. Mesures d’accélération et système d’acquisition par microcontrôleur Arduino UNO. Tech. rep., Polytechnique Montréal. oai: [hal-02018248](#).
- [12] Von Groll, G., and Ewins, D. J., 2001. “The harmonic balance method with arc-length continuation in rotor/stator contact problems”. *Journal of Sound and Vibration*, **241**(2), pp. 223–233. doi: 10.1006/jsvi.2000.3298 - oai: [hal-01333704](#).
- [13] Detroux, T., Renson, L., Masset, L., and Kerschen, G., 2015. “The harmonic balance method for bifurcation analysis of large-scale nonlinear mechanical systems”. *Computer Methods in Applied Mechanics and Engineering*, **296**, pp. 18–38. doi: 10.1016/j.cma.2015.07.017 - oai: [arXiv:1604.05621](#).
- [14] Cameron, T., and Griffin, J., 1989. “An alternating frequency/time domain method for calculating the steady-state response of nonlinear dynamic systems”. *Journal of Applied Mechanics*, **56**(1), pp. 149–154. doi: 10.1115/1.3176036 - oai: [hal-01333697](#).
- [15] Seydel, R., 2009. *Practical bifurcation and stability analysis*, Vol. 5. Springer Science & Business Media. ISBN : 978-1-4419-1739-3.